Int. J. Heat Mass Transfer. Vol. 34, No. 1, pp. 291–303, 1991
Printed in Great Britain

0017–9310/91 $3.00 + 0.00

Theoretical and experimental study of natural convection pipe flows at high Rayleigh number

W. M. YAN and T. F. LIN
Department of Mechanical Engineering, National Chiao Tung University, Hsinchu, Taiwan 30050, R.O.C.

(*Received* 26 *April* 1989 *and in final form* 21 *March* 1990)

Abstract—A combined theoretical and experimental study is performed to investigate natural convection pipe flows at high Rayleigh number. The wall conduction effects and thermal property variations of the fluid and pipe wall are also considered in the analysis. A low-Reynolds-number k–ε turbulence model is employed to treat the transitional and turbulent flow regime including buoyancy effects. The predicted and measured distributions of wall temperature and Nusselt number are in good agreement. Empirical correlations for the induced flow rate and average Nusselt number are proposed. Results show that the characteristics of natural convection heat transfer in a vertical pipe approach those along a single vertical plate for large Rayleigh number.

1. INTRODUCTION

NATURAL convection is the easiest and most inexpensive way to cool the internal surfaces of vertical open-ended ducts and of tube banks, despite the low rates of heat transfer that this convection process affords. Thus information on the behaviour of natural-convection flow through confined spaces has been found useful especially in the thermal-fluid systems encountered in the diverse fields of nuclear and solar energy. Due to its importance, the natural convection problem has received increasing attention in the literature in the past two decades. These studies, however, have mainly restricted their consideration to laminar natural convection flows. Despite the fact that turbulent natural convection in a vertical channel is relatively important in engineering applications, it has not yet received much attention because of its complexity. Eckert and Diaguila [1] performed a pioneering study of turbulent natural convection flows in a vertical channel. In their experimental studies, a small length-to-diameter pipe was used with its wall kept at a uniform and constant temperature. Their results showed that in the laminar range, the measured heat transfer coefficients were higher than the values computed by the local Nusselt number relation for a vertical flat plate. In the turbulent range, however, the mean value of the data was displaced below the curve for the local Nusselt number relation for a single vertical flat plate by approximately 35%. Recently, Miyamoto *et al.* [2] conducted an experimental study on turbulent free convection heat transfer to air drawn between two vertical parallel plates, composed of an adiabatic plate and a plate with uniform heat generation. The transitional phenomena from laminar to turbulent flows were present in their results. Their results also showed that heat transfer characteristics in the vertical plane channel approach those along a single vertical flat plate as the channel separation is enlarged.

Borgers and Akbari [3] were the first to make predictions of turbulent natural convection heat transfer in flows between vertical parallel plates. In their studies, the fluid flow at the channel entrance was assumed to be laminar until a given turbulent criterion is reached, and the flow is assumed to abruptly become fully turbulent. But according to the experimental results obtained for natural convection on a single vertical plate by Godaux and Gebhart [4] and Mahajan and Gebhart [5], the transition from laminar to turbulent flows is a gradual and long process. Therefore, the adoption of a switch criterion beyond which the flow becomes fully turbulent is questionable. Moreover, the use of the mixing-length model for forced convection flows in their computations of turbulent natural convection is also unreliable.

The purpose of this work is to study natural convection pipe flows at high Rayleigh number. Also, an experimental system is established to check the prediction results. The system to be examined theoretically and experimentally is a vertical, open-ended pipe with length l and inner radius R_i (shown schematically in Fig. 1). The pipe wall is subjected to a uniform heat flux q''_w. As a result of the heat transfer to air in the pipe, the temperature of the air increases. The resulting density nonuniformity causes the air in the pipe to rise. The air that enters the vertical channel from the bottom is assumed to be laminar until a combination of geometry, temperature and flow rate conditions reaches a pre-defined level. Beyond that the flow gradually becomes intermittent. The level of the intermittency grows as the flow gradually evolves into the fully turbulent region. The transport processes in this particular region are treated by utilizing the concept of intermittency which has been adopted to solve transitional forced convection flows [6].

NOMENCLATURE

A	cross-sectional area of the pipe
B_b	criterion for beginning of transition, equation (1)
B_e	criterion for end of transition, equation (2)
c_p	specific heat
c_1, c_2, c_μ	constants appearing in k–ε turbulence model
f_1, f_2, f_μ	functions appearing in k–ε turbulence model
Gr^*	Grashof number, $g\beta q''_w R_i^5/(l\lambda\nu_0^2)$
Gr_x^*	Grashof number, $g\beta q''_w x^4/(\lambda\nu_0^2)$
g	gravitational acceleration
h	heat transfer coefficient, $q''_c/(T_w - T_0)$
I	electric current
k	turbulent kinetic energy
l	channel length
Nu	local Nusselt number based on inner radius, hR_i/λ
p	pressure of the air in the channel
p_m	motion pressure (or pressure defect), $p - p_0$
p_0	ambient pressure
q''_c	convection heat flux from the pipe wall to the air, equation (15)
q''_w	energy flux on the wall
Q_c	electrical dissipated heat transfer rate in the pipe wall, equation (22)
r	coordinate in the radial direction
Ra^*	Rayleigh number, equation (27)
Re	Reynolds number based on diameter
R_i	inner pipe radius
R_o	outer pipe radius
R_t	turbulence Reynolds number, $k^2/(\nu\varepsilon)$
t	pipe thickness
T	temperature
T_0	inlet temperature
T_w	wall temperature
u	axial velocity
u_0	inlet axial velocity
$\overline{u'T'}$	longitudinal turbulent heat flux, equation (12)
v	transverse velocity
$\overline{v'T'}$	transverse turbulent heat flux
x	coordinate in the flow direction
y	coordinate in the transverse direction.

Greek symbols

α	thermal diffusivity
β	thermal expansion coefficient, $1/T_0$
γ	turbulent intermittency
ε	rate of dissipation of turbulent kinetic energy
λ	molecular thermal conductivity
λ_w	thermal conductivity of the pipe wall
μ	molecular dynamic viscosity
μ_{eff}	effective viscosity, $\mu + \mu_t$
ν	molecular kinematic viscosity
ν_t	turbulent eddy viscosity, equation (13)
ρ	density
ρ_e	electrical resistivity of the test section, equation (22)
σ_k	turbulent Prandtl number for k
σ_T	turbulent Prandtl number for T
σ_ε	turbulent Prandtl number for ε.

Subscripts

a	air
w	condition at the pipe wall
0	at ambient condition.

For natural convection flows, the transition from laminar to turbulent flow has been examined experimentally for a single heated vertical plate in air by Cheesewright [7], Warner and Arpaci [8], and Miyamoto *et al.* [9]; in water by Godaux and Gebhart [4] and Jaluria and Gebhart [10]. In these studies reference was consistently made to the absence of a parameter which characterizes the beginning of a transition to turbulent flow adjacent to a vertical surface. A good discussion of transition was provided by refs. [4–5]. Despite the fact that a single parameter does not describe the event of transition for a single vertical plate, a rough indication of the start of transition in air and water is given by the criterion $5(Gr_x^*/5)^{1/5} = 450$–700, where $Gr_x^* = g\beta q''_w x^4/(\lambda\nu^2)$.

For natural convection in a vertical channel, the behaviour of heat transfer is similar to that along a single vertical plate when the Rayleigh number is increased [1, 2, 11]. This implies that the curvature of the pipe has an insignificant effect on the characteristics of natural convection heat transfer in a vertical pipe. However, at low Rayleigh number, heat transfer in a vertical channel approaches the fully-developed limit [11], that is, the curvature of the pipe has a pronounced effect on the flow behaviour in a vertical pipe. At high flow rates the turbulence is expected to be initiated earlier, that is, the location for the incipience of transition should be inversely related to the induced volumetric flow rate. Therefore, the model employed to describe the transition must have the flexibility to account for these conditions. The criterion used in this work to characterize the beginning of transition accounts for both the Rayleigh number and Reynolds number dependence, and is expressed as

$$Re^{1/2}(Pr\, Gr_x^*)^{1/4} = B_b. \quad (1)$$

This expression is similar to that used by Borgers

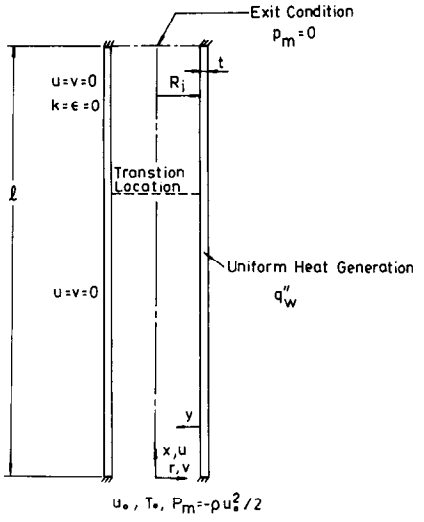

FIG. 1. Schematic diagram of the physical system and the boundary conditions.

and Akbari [3]. Similarly, the end transition point is also indicated by an equation of the same form

$$Re^{1/2}(Pr\,Gr_x^*)^{1/4} = B_e \tag{2}$$

where the constants B_b and B_e are respectively chosen to be 1.5×10^5 and 2.0×10^5 so as to make the predicted results closer to our experimental data and make the trends of the predicted results closer to those in related works [1, 2].

Notice that the above transitional criteria, equations (1) and (2), hold only as the induced Reynolds number at the inlet, Re, is greater than the critical Reynolds number, Re_{crit}, at which the forced convection channel flow becomes transitional. The value of Re_{crit} in a pipe flow is taken as 2300.

Because the intermittency concept is used to describe the transition from laminar to turbulent flow, it may be reasonably assumed that the effective viscosity is calculated by weighting the laminar (molecular) viscosity by the time period during which the flow is laminar (i.e. $1-\gamma$) and by weighting the effective turbulent viscosity by the time period during which the flow is turbulent (i.e. γ). Thus one has

$$\mu_{eff} = (1-\gamma)\mu+\gamma(\mu+\mu_t). \tag{3}$$

The intermittency factor γ is set to zero when the flow is laminar, i.e. when $Re^{1/2}(Pr\,Gr_x^*)^{1/4} \leqslant B_b$. Similarly, for $Re^{1/2}(Pr\,Gr_x^*)^{1/4} \geqslant B_e$ the intermittency factor γ is set to 1, i.e. the flow is fully turbulent. During the transition process, γ is assumed to be linear [6]

$$\gamma = (B-B_b)/(B_e-B_b) \tag{4}$$

where

$$B = Re^{1/2}(Pr\,Gr_x^*)^{1/4}. \tag{5}$$

2. ANALYSIS

The analysis is based on a model consisting of convection heat transfer in the vertical pipe coupled with conduction heat transfer in the pipe wall. Attention is focused on the governing equations for the natural convection heat transfer in an open ended vertical pipe.

2.1. *The convection problem*

With the boundary layer approximations, the steady, time averaged governing equations are:

continuity equation

$$\frac{\partial}{\partial x}(r\rho u)+\frac{\partial}{\partial r}(r\rho v) = 0; \tag{6}$$

axial-momentum equation

$$\rho u\frac{\partial u}{\partial x}+\rho v\frac{\partial u}{\partial r} = \frac{1}{r}\frac{\partial}{\partial r}\left[r(\mu+\mu_t)\frac{\partial u}{\partial r}\right] - \frac{dp_m}{dx}+(\rho_0-\rho)g; \tag{7}$$

energy equation

$$\rho c_p u\frac{\partial T}{\partial x}+\rho c_p v\frac{\partial T}{\partial r} = \frac{1}{r}\frac{\partial}{\partial r}\left[r(\lambda+\lambda_t)\frac{\partial T}{\partial r}\right]. \tag{8}$$

Notice that the thermophysical properties of the fluid are considered as variable with temperature because large temperature variation in the flow is expected. The turbulent viscosity μ_t is computed in accordance with the k–ε turbulence model. Hence the transport equations for the turbulent kinetic energy and its dissipation must be included in the analysis. To procure more reliable results, a low-Reynolds number k–ε model is selected to eliminate the usage of wall functions in the computations and thus to permit direct integration of the transport equations to the channel wall.

The turbulent kinetic energy equation is

$$\rho u\frac{\partial k}{\partial x}+\rho v\frac{\partial k}{\partial r} = \frac{1}{r}\frac{\partial}{\partial r}\left[r\left(\mu+\frac{\mu_t}{\sigma_k}\right)\frac{\partial k}{\partial r}\right]+\mu_t\left(\frac{\partial u}{\partial r}\right)^2 - \rho\varepsilon-2\mu\left(\frac{\partial k^{1/2}}{\partial r}\right)^2+|\rho g\beta\overline{u'T'}| \tag{9}$$

and the rate of dissipation of turbulent kinetic energy is determined from the equation

$$\rho u\frac{\partial \varepsilon}{\partial x}+\rho v\frac{\partial \varepsilon}{\partial r} = \frac{1}{r}\frac{\partial}{\partial r}\left[r\left(\mu+\frac{\mu_t}{\sigma_\varepsilon}\right)\frac{\partial \varepsilon}{\partial r}\right] + c_1 f_1\frac{\varepsilon}{k}\mu_t\left(\frac{\partial u}{\partial r}\right)^2-c_2 f_2\rho\frac{\varepsilon^2}{k}+2\frac{\mu\mu_t}{\rho}\left(\frac{\partial^2 u}{\partial r^2}\right) + \left|c_1\frac{\varepsilon}{k}\rho g\beta\overline{u'T'}\right|. \tag{10}$$

It is worth noting that the molecular viscosity is

also included in the k–ε equations. This molecular viscosity is particularly important in the region near the wall [12, 13]. In the above equations the density fluctuation correlations are ignored except in the buoyancy production terms in the k and ε equations [14, 15].

Equations for the turbulence variables, k and ε, are solved numerically only in the computational subdomain bounded by the transition plane, downstream boundary, and pipe wall, as shown in Fig. 1. In the present study the flow flowing in the initial portion of the channel is assumed to be laminar until the transition condition, equation (1), is reached. To initiate the turbulence computation, a small amount of kinetic energy of turbulence ($k_{in} = 1.5 \times 10^{-4} u_0^2$) was introduced at the transition plane [16]. In addition, at this plane it is assumed that $\varepsilon = c_\mu f_u k^2$. Equations (6)–(10) are to be solved with the following boundary conditions:

$$x = 0, \quad u = u_0, \quad T = T_0, \quad p_m = -\rho u_0^2/2 \tag{11a}$$

$$r = 0, \quad \partial u/\partial r = 0, \quad \partial T/\partial r = 0,$$

$$\partial k/\partial r = 0, \quad \partial \varepsilon/\partial r = 0 \tag{11b}$$

$$r = R_i, \quad u = 0, \quad \lambda \partial T/\partial r = q_c''(x), \quad k = 0, \quad \varepsilon = 0 \tag{11c}$$

$$x = l, \quad p_m = 0 \tag{11d}$$

where $q_c''(x)$ is the convection heat flux from the pipe wall to the fluid.

For the specific geometry of the pipe and the heating condition, there exists only a unique value of the inlet velocity u_0 which yields $p_m = 0$ at the pipe exit. In the numerical calculation procedures utilized in the present study, this value of u_0 was obtained iteratively, as will be described later.

In equations (9) and (10), the low-Reynolds-number k–ε turbulence model proposed by Jones and Launder [12, 13] was modified by adding terms representing the contribution of the buoyancy force to the turbulent kinetic energy and its dissipation rate. Under the gradient assumption in the k–ε model, $g\beta\overline{u'T'}$ is proportional to $-\partial T/\partial x$ and, as a result, means a destruction, albeit small, of turbulent kinetic energy. This is contrary to the usual concept that the term $g\beta\overline{u'T'}$ is a production term [9, 17]. Because the inconsistency arises as a result of assuming $g\beta\overline{u'T'} \propto -\partial T/\partial x$, Mason and Seban [18] and Markato *et al.* [14] took $g\beta\overline{u'T'}$ to be $g\beta\overline{v'T'}$ and modelled it as

$$g\beta\overline{u'T'} = g\beta \frac{\nu_t}{\sigma_T} \cdot \frac{\partial T}{\partial r}. \tag{12}$$

No justification, other than the fact that the correct sense of the gradient assumption is not preserved. Fortunately, we found that, at least for air, this contribution to k had a negligible effect on their numerical results. In the present study this term is retained and is modelled in accordance with Mason and Seban [18].

In the governing equations the turbulent eddy viscosity for momentum, μ_t, is related to k and ε by

$$\mu_t = \rho c_\mu f_u (k^2/\varepsilon). \tag{13}$$

The appropriate constants and turbulent Prandtl numbers, σ_k and σ_ε, as well as the low-Reynolds-number wall damping functions, f_u and f, are not known at the present time for turbulent natural convection flows, although they have been generated and optimized for forced convection flows [12, 13, 19]. For lack of a better choice, these results for forced convection flows are retained in the present analysis for natural convection. These values and functions are listed in Table 1.

One constraint to be satisfied in the analysis of a steady channel flow is the overall mass balance at every axial location in the pipe. It is

$$\int_0^{R_i} \rho u 2\pi r \, dr = \rho_0 u_0 \pi R_i^2. \tag{14}$$

This equation is used in the solution process to deduce the pressure gradient in the flow.

2.2. *The conduction problem*

In the present study, consideration is given here to pipes with a relatively thin wall so that the temperature variations across the thickness of the wall can be neglected. To simulate the experimental heating condition, a d.c. electric current is passed through the pipe wall. Taking a lumped control volume, the wall energy balance becomes

$$\frac{d}{dx}\left(\lambda_w \frac{dT}{dx}\right) t + q_w'' - q_c'' = 0 \tag{15}$$

where t is the thickness of the pipe wall and q_w'' the heat flux generated by the resistance heating in the pipe wall.

The boundary conditions for equation (15) are

$$x = 0, \quad dT_w/dx = 0 \tag{16a}$$

$$x = l, \quad dT_w/dx = 0. \tag{16b}$$

Note that at the fluid–wall interface, the temperature and heat flux should be continuous.

3. SOLUTION METHOD

Solution of the conjugate problem defined by the foregoing equations is obtained numerically by a finite difference method. In view of the fact that the boundary conditions have to be satisfied at both the upstream and downstream ends of the pipe, an iteration approach is used, with the discretized governing equations for the convection and conduction problems being solved simultaneously. A fully-implicit numerical scheme in which the axial convection is approximated by the upstream difference, and radial convection and diffusion terms by the central difference is employed to transform the governing equa-

Table 1. The constants and the functions

c_1	c_2	c_μ	f_1	f_2	f_μ	σ_T	σ_k	σ_ε	R_t
1.45	2.0	0.09	$1-0.15e^{-(R_t/50)^2}$	$1-0.3e^{-R_t^2}$	$e^{-2.5/(1+R_t/50)}$	0.9	1.0	1.3	$k^2/(\nu\varepsilon)$

tions into finite-difference equations. Each system of finite-difference equations forms a tridiagonal matrix equation which can be solved by the Thomas algorithm [20]. For a given condition, a brief outline of the solution procedure is as follows:

(1) Guess the inlet velocity u_0 and pipe wall temperature T_w ($x = 0$).

(2) For any axial location, guess (dp_m/dx) and solve the finite-difference form of equations (7), (8) and (15) for u and T.

(3) Integrate the continuity equation numerically to find v

$$v = \frac{-1}{\rho \cdot r}\frac{\partial}{\partial x}\int_0^r \rho u r \, dr. \tag{17}$$

(4) Check whether the transition is reached. If it is, solve the finite-difference forms of equations (9), (10) and (13) for k, ε and μ_t. If not, skip to the next step.

(5) Check the satisfaction of the overall conservation of mass, equation (14). If it is satisfied to within a specified tolerance, repeat the above procedure for the next axial location. In the present study the tolerance of overall conservation of mass is 10^{-4}. If not, guess a new (dp_m/dx) by the Newton–Raphson method and repeat procedures (2)–(5) for the current location.

(6) Procedures (2)–(5) are successively applied to every axial location from the pipe entrance to the exit.

(7) Employ extrapolation to evaluate the pipe wall temperature at $x = 0$.

(8) Check the convergence of u and T and check whether the exit pressure p_m is equal to zero. If both conditions are not simultaneously satisfied, guess a new inlet velocity u_0 by the Newton–Raphson method and repeat procedures (2)–(8). If both conditions are satisfied, the solution is complete. Note that the detailed convergence criteria for the various variables are available in ref. [21].

In the solution of finite-difference equations by the Thomas algorithm, a successive under-relaxation numerical scheme is used. It is found that the computer time can be reduced by as much as 20% if the under-relaxation factor for u, T, k and ε are selected to be 0.7 and 0.3 for p_m.

The heat transfer coefficient, a parameter of major interest in the study of convection heat transfer, can be evaluated by

$$h = \frac{q_c''}{T_w - T_0} \tag{18}$$

where q_c'' is the convection heat flux from the pipe wall to the air in the pipe. The local Nusselt number, based on the local channel length x, is defined as

$$Nu_x = \frac{hx}{\lambda} \tag{19}$$

and another local Nusselt number, based on the pipe radius R_i, is defined as

$$Nu = \frac{hR_i}{\lambda}. \tag{20}$$

It is worth noting that the local Nusselt number is based on $(T_w - T_0)$, rather than on $(T_w - T_m)$ [11]. This is because the bulk temperature T_m is difficult to measure in the experiment.

4. EXPERIMENTAL STUDY

4.1. *Experimental apparatus and description*

In the present study, the test section is made of stainless steel SS304 circular pipe. Several pipes of different diameter, thickness and length are employed. Electric power is supplied by a d.c. rectifier with an a.c. input of 220 V, 3ϕ and an output range of voltage 0–60 V and current 0–1000 A. The electric power is dissipated in the test section, which acts as a resistance element and ensures nearly uniform heat generation along the test section. Copper electrodes are wound around the pipe ends of the test section. In order to reduce the heat loss from the test section to the ambient, the test section is covered with balsawood insulators. To obtain the temperature distributions in the air flow, four traversing mechanisms were employed to measure the radial temperature variations at various axial locations.

4.2. *Experimental technique*

4.2.1. *Measurement of wall temperature.* The outer wall temperatures at several locations of the test section are measured by 21 T-type (copper–constantan) thermocouples (0.3 mm). The thermocouple locations along the pipe are equally spaced in the flow direction. The first and final thermocouples are respectively fixed at the pipe ends. At three axial locations along the test section designated as numbers 4, 10 and 16, three thermocouples are fixed equidistantly around the circumference of the pipe to check the circumferential uniformity of the wall temperature.

The inside wall temperatures at the measuring locations are estimated from the measured outer wall temperature from the steady-state heat conduction solution for a hollow cylinder with a uniform internal

heat generation and the outer wall being well insulated. The result is

$$T'_w - T_w = \frac{Q_e}{2\pi(R_o^2 - R_i^2)\lambda_w l}\left[R_o^2 \ln(R_o/R_i) - \frac{R_o^2 - R_i^2}{2}\right] \quad (21)$$

where Q_e is the total heat input to the test section, and R_o and R_i are the outer and inner radii of the pipe, respectively.

4.2.2. *Measurement of heat flux.* The electric power input to the test section is determined from the measured voltage drop across the test section and the current along the test section

$$Q_e = IV = I^2 \frac{\rho_e l}{\pi(R_o^2 - R_i^2)} \quad (22)$$

where I and V are electric current and voltage and ρ_e the electrical resistivity of the test section.

Heat loss by natural convection from the test section through the insulation is evaluated by measuring the outer surface temperature of the insulation and the ambient temperature. With these data a standard correlation can be used to estimate the heat loss. At seven axial locations along the pipe the outer surface temperatures of the insulator are measured by T-type thermocouples, and the average (arithmetic) insulation temperature T_{ins} is determined. The heat loss q''_{loss} is then computed by the suggested correlation for natural convection from a vertical cylinder in air [22].

The heat loss q''_{loss} is taken into account in computing the average wall heat flux in the test section q''_w. In this connection, the local wall heat flux can be obtained from the average wall heat flux and a correction factor accounting for the variation of the resistivity of the tube material in conjunction with the calculated local wall temperature. The relation is given by

$$q''_{w,i} = q''_w \rho_e(T_w)/\rho_e(\bar{T}_w). \quad (23)$$

With the measured local wall temperature and the local generated heat flux, the local Nusselt number can then be evaluated by

$$Nu = \frac{q''_c}{(T_w - T_0)\lambda/R_i} \quad (24)$$

where the local convective heat flux q''_c can be obtained from equation (15).

4.3. *Uncertainty analysis*

The purpose of performing the uncertainty analysis was to estimate the uncertainty levels in the measured Nusselt number and Rayleigh numbers. The uncertainty levels obtained from such analysis were compared to the scatter displayed by the measured data in order to evaluate their reliability. Also, the levels of the uncertainty in $\overline{Nu}$ and Ra^* were to provide appropriate basis for future comparison with those from other investigations.

In the analysis only the random components of the experimental uncertainties were taken into account since the fixed part of the uncertainties were considered comparatively negligible [23]. Kline and McClintock [24] proposed a formula for evaluating the uncertainty in the result F as a function of the independent variables, $v_1, v_2, \ldots, v_n$

$$F = F(v_1, v_2, \ldots, v_n) \quad (25)$$

the uncertainty in F is expressed by

$$\delta F = \left[\left(\frac{\partial F}{\partial v_1}\delta v_1\right)^2 + \left(\frac{\partial F}{\partial v_2}\delta v_2\right)^2 + \cdots + \left(\frac{\partial F}{\partial v_n}\delta v_n\right)^2\right]^{1/2} \quad (26)$$

where $\partial F/\partial v_i$ and δv_i are, respectively, the sensitivity coefficient and the uncertainty level associated with the variable v_i. The values of the uncertainty intervals δv_i were obtained by an r.m.s. combination of the precision uncertainty of the instruments (one-half of the smallest scale division) and the unsteadiness uncertainty (i.e. two standard deviations of a set of repeated observations of the value v_i), as recommended by ref. [23]. The choice of the variables v_i to be included in the calculation of the total uncertainty level of the result F depends on the purpose of the analysis. If the calculated uncertainty level is to be compared to the scatter of the experimental data, variables like dimensions of the test section or fluid properties should not be included (First Order Analysis, according to Moffat [23]). On the other hand, for the reporting of the data and for the comparison of results with analytic or numerical solutions, the effects of the uncertainty in all variables influencing the result F should be taken into account (Nth Order Analysis, according to ref. [23]). The detailed results of the uncertainty analysis are summarized in the Appendix. The nominal values and uncertainty intervals for the main contributing variables are shown in Table A1 in the Appendix. As shown in that table, the resulting uncertainty in $\overline{Nu}$ ranges from 4.40 to 5.53%. In performing the uncertainty analysis, it was found that the largest individual contribution to the uncertainties in $\overline{Nu}$ and Ra^* came from the uncertainty of the convection heat flux q''_c and the uncertainty of the pipe wall radius R_i. The detailed description on the uncertainty analysis was available in ref. [21].

5. RESULTS AND DICUSSION

In the present study, particular attention is paid to examining the distributions of convective heat transfer coefficient at high Rayleigh number. To conveniently discuss the results, the results from the numerical prediction are first presented. After these,

Table 2. Values of major parameters for various cases

Case	l (m)	R_i (m)	q''_w (W m^{-2})	t (m)	Ra^*	Pr
I	4	0.12	80	0.002	1.77×10^6	0.707
II	4	0.08	80	0.002	2.33×10^5	0.707
III	4	0.08	40	0.002	1.16×10^5	0.707
IV	4	0.04	80	0.002	7.27×10^3	0.707
V	4	0.04	40	0.002	3.64×10^3	0.707
VI	2	0.04	80	0.002	1.45×10^4	0.707
VII	2	0.04	40	0.002	7.27×10^3	0.707
VIII	2	0.02	40	0.002	2.27×10^2	0.707

the measured data are illustrated and contrasted with the numerical predictions.

5.1. *Numerical results*

Numerical solutions of the governing equations with the associated boundary conditions are obtained for wide ranges of pipe length, pipe radius and wall heating levels q''_w. The conditions for all the cases selected for the numerical computations are listed in Table 2. In this work, the governing non-dimensional parameters are given below:

$$Ra^* = g\beta q''_w R_i^5/(l\nu_0\alpha_0\lambda_0)$$

$$Ra^*_x = g\beta q''_w x^4/(\nu_0\alpha_0\lambda_0)$$

$$Gr^* = Ra^*/Pr$$

$$Pr = \nu_0/\alpha_0. \qquad (27)$$

A systematic literature search has not revealed any available experimental and theoretical data with which the results of this computation may be directly compared. To check the adequacy of the numerical scheme and turbulence model described above, the limiting case of turbulent mixed convection between vertical parallel plates was first obtained by the present prediction. The predicted results are in good agreement with the experimental data of Nakajima *et al.* [25]. The detailed comparison was given in ref. [26]. Furthermore, special care was taken to establish the arrangement of gridlines required to produce essentially grid-independent results. A total of 101×61 gridlines was placed in the x- and r-directions, respectively. Computations with finer grid size showed that the local Nusselt number changed less then 3% with a doubling of the gridlines. This lends support to the employment of the turbulence model and the numerical scheme proposed to the analysis of the present problem.

In this study, we are concerned with natural convection flow in a vertical pipe at high Rayleigh number. As is expected, the results will approach those along a single vertical, heated plate as the pipe radius R_i is large or as $Ra^* \to \infty$. In this connection the predicted results for a large R_i can be qualitatively compared with the published results for a single vertical plate. It is worth noting that as the Rayleigh number is small, the induced flow is laminar instead of turbulent. Therefore, the predicted results are essentially identical to those of Pollard and Oosthuizen [27].

Figure 2 gives the distributions of the local Nusselt number Nu_x along the channel wall from the present prediction for various pipe radii and their comparisons with the known relations for a single vertical plate. Evidently from the figure, the predicted values in the laminar regime are slightly above the curve for the corresponding laminar local Nusselt number relation for a single vertical flat plate [28]. In the turbulent range, the opposite trend is observed, that is, the predicted results are displaced below the curve for the corresponding local turbulent Nusselt number relation for a vertical flat plate. The discrepancy between the predicted results and the relations for a vertical plate decreases with increasing pipe radius for the value considered. This confirms the fact that the natural convection heat transfer processes in a vertical pipe with a large radius are close to those along a vertical plate [1, 2, 11, 16].

Shown in Fig. 3 are the wall temperature distributions for various pipe radii and wall heat fluxes with $l = 4$ m. An overall inspection of this plot reveals that near the entrance (i.e. small x/l), the wall temperature increases with x/l. But beyond certain locations downstream the wall temperature decreases and then increases again. This non-monotonic variation in T_w can be made plausible by noting the fact that near the entrance, the flow is laminar and the

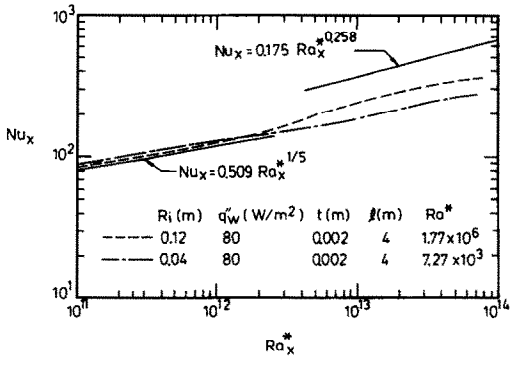

FIG. 2. Distributions of local Nusselt number and comparison with known equations for single vertical plate.

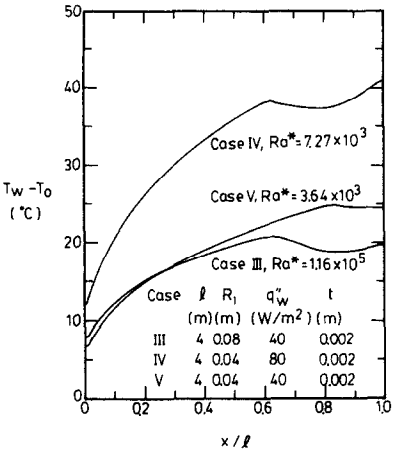

FIG. 3. Predicted wall temperature distributions along the pipe.

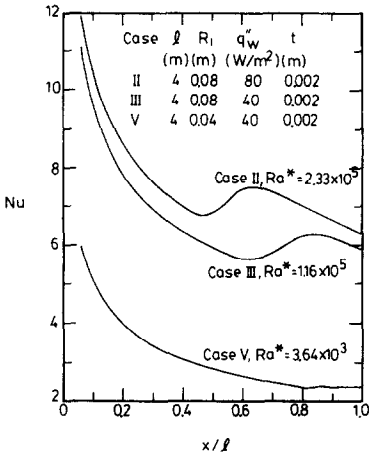

FIG. 5. Calculated Nusselt number distributions along the pipe for $l = 4$ m.

wall temperature increases with x due to wall heating. But as the flow goes downstream, the flow becomes unstable and transitional. Thus heat transfer is more effective in this transitional stage, which, in turn, results in a decreasing T_w. After this transitional stage, the flow becomes fully turbulent. Thus the heat transfer coefficient gradually decreases with x and the corresponding wall temperature increases with x. The above features are similar to those found by Miyamoto *et al.* [2]. Comparing the results for cases III and V indicates that near the entrance ($x/l < 0.2$) the higher wall temperature is experienced for the case with a larger pipe radius (case III). But as the flow moves further downstream, the opposite trend is noted. Moreover, the location of transition is closer to the channel entrance for the case with a larger R_i. Also included in Fig. 3 are the influence of wall heat flux on the distributions of wall temperature.

In the study of natural convection, the convection heat transfer coefficient is one of the major parameters in understanding heat transfer characteristics in the flow. In order to examine the effects of the pipe length on the flow transition and heat transfer, the local Nusselt number Nu for $l = 2.0$ and 4.0 m at different conditions are, respectively, illustrated in Figs. 4 and 5. In Fig. 4, the local Nusselt number monotonically decreases with x. In these cases the flow in the channel is entirely laminar and no flow transition occurs. Focusing on the results at the same x/l indicates that a larger local Nusselt number is experienced for the case with a higher Rayleigh number Ra^*. This confirms the general perception that in natural convection channel flow heat transfer is more effective for a system with a higher Ra^*.

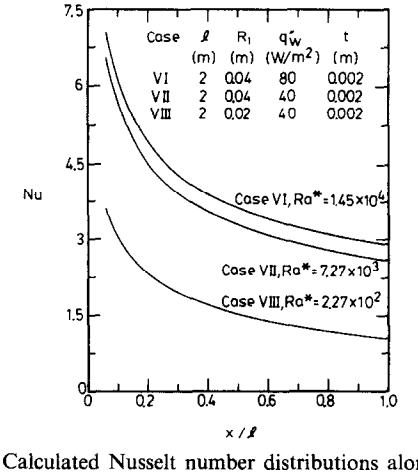

FIG. 4. Calculated Nusselt number distributions along the pipe for $l = 2$ m.

For pipe length $l = 4$ m (Fig. 5), the flow near the entrance is still laminar and Nu decreases with x due to the entrance effect. But further downstream, the natural convection flow near the heated pipe wall becomes unstable. Through a series of complicated mechanisms of linear and non-linear interactions, the flow becomes fully turbulent. In the transitional stage the heat transfer coefficient increases with x. As the flow becomes fully turbulent, the augmentation in heat transfer stops. Instead, Nu gradually decreases. It is found from Fig. 5 that the location of transition is shifted downstream as R_i decreases (by comparing cases III and V). The delay of flow transition in a pipe with a small R_i may result from the fact that the flow would experience a large viscous resistance when it passes through a smaller pipe. Moreover, the transition is initiated earlier for the case with a higher q''_w (by comparing cases II and III). Also found in Fig. 5 are the larger local Nusselt numbers for the flow in a larger pipe.

The buoyancy induced volume flow rate through the vertical open pipe is important in many industrial applications. Figure 6 presents the variations of Reynolds number Re, which is based on the pipe diameter and inlet average velocity, with the pipe length. It is observed in this plot that a higher Reynolds number is experienced for the case with a longer pipe. Reynolds number Re increases significantly with l when the channel is short. As the channel gets longer, Re only gradually increases. Comparison of the curves for cases IV and V indicates that the higher the wall heat flux, the higher the Reynolds number. This is simply

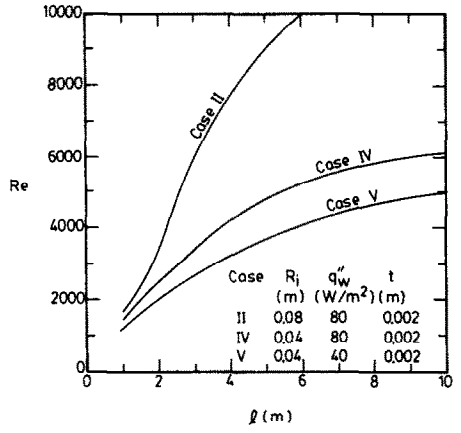

FIG. 6. Effects of pipe length on the induced volume flow rate.

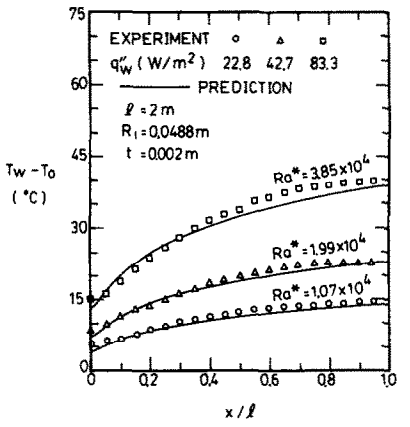

FIG. 8. Local wall temperature distributions for $l = 2$ m, $R_i = 0.0488$ m and $t = 0.002$ m.

due to the larger buoyancy effects for a higher wall heat flux.

It is more useful in applications if the curves in Fig. 6 for different conditions can be collapsed into a single curve. Figure 7 presents the variations of dimensionless volume flow rate Q^* with Ra^*. Q^* is defined as

$$Q^* = \frac{\pi R_i^2 u_0}{l\nu_0 Gr^*} = \frac{\pi}{2}\frac{Re}{Gr^* \cdot l/R_i}. \tag{28}$$

In the computations, the predicted volume flow rate Q^* for different cases always lies on a straight line in a log–log plot. This interesting result is also observed by Miyamoto *et al.* [2] in the study of turbulent natural convection between vertical parallel plates. Therefore, a straight line is used to fit the predicted results, as shown by the solid line in Fig. 7. The relation is

$$Q^* = 1.507 Ra^{*-0.62}. \tag{29}$$

5.2. *Experimental results*

Now we turn attention to examining the experimental results. As mentioned earlier, the main objective of this study is to investigate natural convection heat transfer at high Rayleigh number. To this end, a variety of test sections with large pipe sizes (i.e. long pipe length and large pipe radius) is employed in the experimental runs.

Figures 8–13 give the measured wall temperature and Nusselt number distributions for different pipe sizes and wall heat fluxes. For comparison purposes, the predictions from the theoretical model are also included in these plots. The experimental data are represented by different symbols, corresponding to different wall heating conditions. The solid lines are from our numerical predictions. First, we focus attention on the results in Figs. 8 and 9 for the system with length $l = 2$ m, radius $R_i = 0.0488$ m and thickness $t = 0.002$ m. Clearly, the numerical predictions basically agree with the experimental data. An inspection of Fig. 8 discloses that the wall temperature increases monotonically with the axial location x/l. No temperature drop occurs. This implies that in these experimental runs no flow transition exists in the channel. Moreover, the larger the wall heat flux (Rayleigh number Ra^*), the higher the wall temperature. Notice that at $x/l = 0$ the wall temperature is higher than the ambient temperature, especially for the case with a

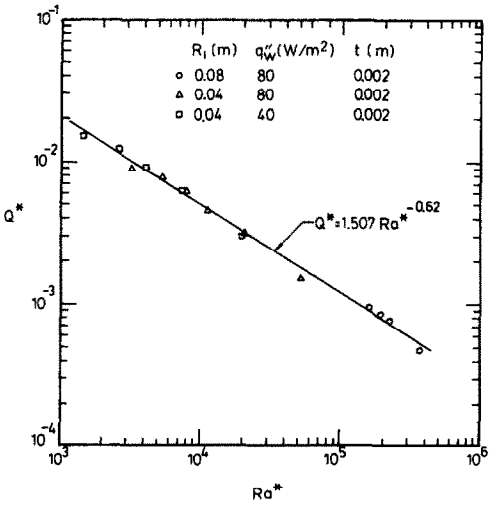

FIG. 7. Dimensionless induced volume flow rate against Rayleigh number.

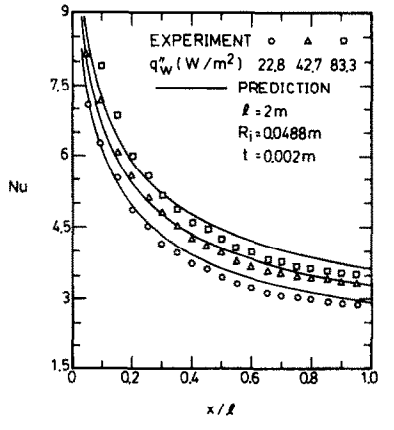

FIG. 9. Axial distributions of Nusselt number for $l = 2$ m, $R_i = 0.0488$ m and $t = 0.002$ m.

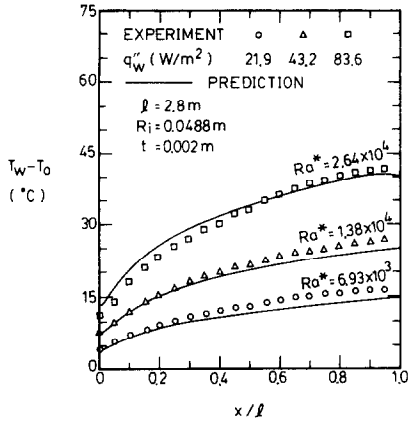

FIG. 10. Local wall temperature distributions for $l = 2.8$ m, $R_i = 0.0488$ m and $t = 0.002$ m.

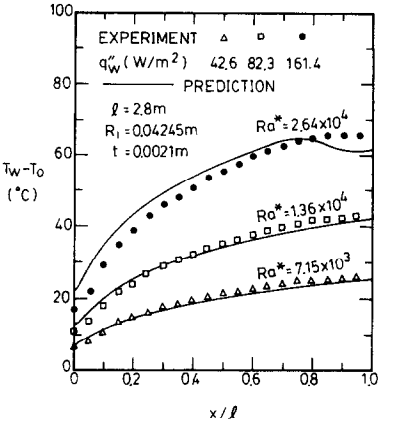

FIG. 12. Local wall temperature distributions for $l = 2.8$ m, $R_i = 0.0425$ m and $t = 0.0021$ m.

high wall heat flux. This is simply due to axial heat conduction in the pipe wall.

In Fig. 9 the local Nusselt number Nu decreases with x/l owing to the entrance effect. Additionally, larger Nusselt number is experienced for the case with a higher q''_w (or Ra^*). This confirms the fact that heat transfer in buoyancy-driven channel flow is more effective for the case with a larger Ra^*. Careful scrutiny of this plot reveals that near the entrance the numerical calculation underpredicts the experimental data while in the downstream region the Nusselt number is overpredicted. These differences may be partially due to the experimental uncertainties.

Attention is now turned to the effects of pipe length on the natural convection heat transfer. Figures 10 and 11 are the experimental results along with the predicted results for $l = 2.8$ m. Comparing the corresponding curves in Figs. 9 and 11 shows that at the same x/l, smaller Nu is observed for the longer pipe. This is again due to the fact that a longer pipe gives a smaller Rayleigh number Ra^*, which in turn causes a smaller Nusselt number. It is interesting to note that in Fig. 11 the predicted result for $q''_w = 83.6$ W m^{-2} ($Ra^* = 2.64 \times 10^4$) shows a slight rise in Nu near the outlet. As explained in Fig. 5, the slight rise in Nu is due to the flow transition.

Figures 12 and 13 present the measured results for the system with $l = 2.8$ m, $R_i = 0.04245$ m and $t = 0.0021$ m at different wall heat fluxes. An overall inspection of these two plots shows that the predicted results agree well with the experimental data except for the case with $q''_w = 161.4$ W m^{-2} ($Ra^* = 2.64 \times 10^4$). Notice that in Fig. 12 the predicted T_w for $q''_w = 161.4$ W m^{-2} has a dip near the exit end of the pipe. Again this is due to the flow transition predicted by the transitional criteria just developed. Although the measured wall temperature does not clearly exhibit this transitional region, in the experimental run the temperature of the air flow for $q''_w = 161.4$ W m^{-2} at $x/l = 0.857$ measured by the traversing mechanism indeed shows a fluctuating characteristic with relative temperature intensity as high as 6%. This proves that the air flow at $x/l = 0.857$ is no longer laminar. Instead, the flow is weakly transitional at this location. In order to verify the turbulence and transition models and to understand the characteristics of transition, a further study should be pursued. The above comparison cannot be considered as a direct verification

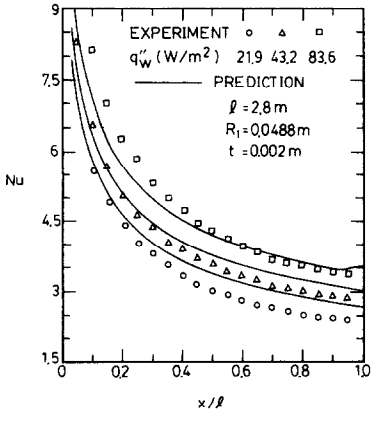

FIG. 11. Axial distributions of Nusselt number for $l = 2.8$ m, $R_i = 0.0488$ m and $t = 0.002$ m.

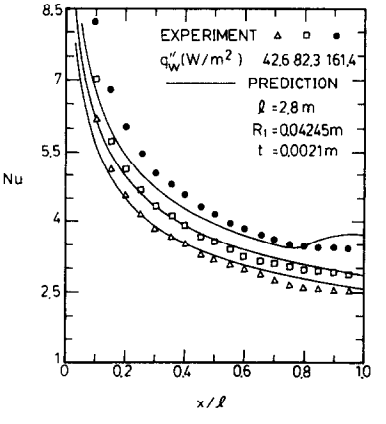

FIG. 13. Axial distributions of Nusselt number for $l = 2.8$ m, $R_i = 0.0425$ m and $t = 0.0021$ m.

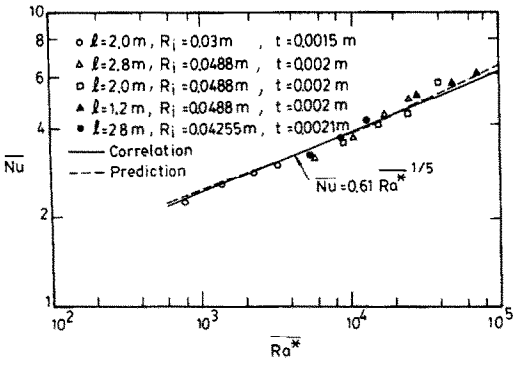

FIG. 14. Average Nusselt number against Rayleigh number.

of the transition and turbulence models developed in Sections 1 and 2, but in the related works [16, 29] similar transition and turbulence models have been used to predict the transitional, turbulent natural convection heat transfer between vertical parallel plates. The predicted results were contrasted with the available data in the literature and showed that excellent agreement was found. Therefore, the transitional and turbulence models used in this work should be qualitatively good. To further ascertain the suitability and adequacy of the transitional model, an experimental study with longer and larger pipes is recommended.

Results for the average Nusselt number $\overline{Nu}$ are particularly useful for the designers of thermal systems. In Fig. 14 $\overline{Nu}$ is plotted against $\overline{Ra}^*$ for different heating conditions and pipe sizes. Notice that the calculations of the physical properties appearing in $\overline{Nu}$ and $\overline{Ra}^*$ are based on the average wall temperature along the channel. The solid line in Fig. 14 represents the correlation of the experimental data. The relation is

$$\overline{Nu} = 0.61\overline{Ra}^{*1/5}. \tag{30}$$

The slope of this line is 1/5, which is in agreement with the results for natural convection over a single vertical plate. In equation (30) $\overline{Nu}$ contains R_i (inner radius) to the first power, $\overline{Nu} = h \cdot R_i/\lambda$, and $\overline{Ra}^*$ is proportional to R_i to the fifth power, equation (27). As a result $\overline{Nu}$ is independent of R_i. This confirms the general perception that at large Rayleigh number natural convection heat transfer in a vertical channel approaches that along a single vertical plate [1, 2, 11].

6. CONCLUSIONS

The natural convection heat transfer in a vertical pipe has been studied theoretically and experimentally. The effects of channel length, pipe radius and imposed wall heat flux on the characteristics of transitional natural convection heat transfer are examined in detail. What follows is a brief summary of the major results:

(1) The characteristics of natural convection heat transfer in a vertical pipe approach those along a single vertical plate for large Rayleigh number Ra^* (or, large pipe radius).

(2) The dimensionless volume flow rate drawn through the pipe decreases with increasing Ra^*. The relations on a log–log plot can be approximated by a straight line for different conditions. The relation is $Q^* = 1.507Ra^{*-0.62}$.

(3) The measured wall temperature and Nusselt number distributions agree well with the predicted results, except for the cases with a high imposed wall heat flux.

(4) In the range of the present experimental study all the measured data for the average Nusselt number can be correlated by one equation, $\overline{Nu} = 0.61\overline{Ra}^{*1/5}$.

Acknowledgement—The financial support of this research by the engineering division of the National Research Council of Taiwan, R.O.C., through the contract NSC76-0401-E009-6 is appreciated.

REFERENCES

1. E. R. G. Eckert and A. J. Diaguila, Experimental investigation of free-convection heat transfer in vertical tube at large Grashof numbers, NACA Report 1211 (1955).
2. M. Miyamoto, Y. Katoh, J. Kurima and H. Sasaki, Turbulent free convection heat transfer from vertical parallel plates, *Proc. 8th Int. Heat Transfer Conf.*, San Francisco, Vol. 4, pp. 1593–1598 (1986).
3. T. R. Borgers and H. Akbari, Free convection turbulent flow within the Trombe wall channel, *Sol. Energy* **33**, 253–264 (1984).
4. F. Godaux and B. Gebhart, An experimental study of the transition of natural convection flow adjacent to a vertical surface, *Int. J. Heat Mass Transfer* **17**, 93–107 (1974).
5. R. L. Mahajan and B. Gebhart, An experimental determination of transition limits in a vertical natural convection flow adjacent to a surface, *J. Fluid Mech.* **91**, 131–154 (1979).
6. T. Cebeci and P. Bradshaw, *Physical and Computational Aspects of Convection Heat Transfer*, pp. 187–188. Springer, New York (1984).
7. R. Cheesewright, Turbulent convection from a vertical plate surface, *J. Heat Transfer* **90**, 1–8 (1968).
8. C. Y. Warner and V. S. Arpaci, An experimental investigation of turbulent natural convection in air at low pressure along a vertical heated flat plate, *Int. J. Heat Mass Transfer* **11**, 397–406 (1968).
9. M. Miyamoto, H. Kajimo, J. Kurima and I. Takamami, Development of turbulence characteristics in a vertical free convection boundary layer, *Proc. 7th Int. Heat Transfer Conf.*, Munich, F.R.G., Vol. 2, pp. 323–328 (1982).
10. Y. Jaluria and B. Gebhart, On transition mechanism in vertical natural convection flow, *J. Fluid Mech.* **66**, 309–337 (1974).
11. E. M. Sparrow and L. F. A. Azevedo, Vertical-channel natural convection spanning between the fully-developed limit and the single-plate boundary-layer limit, *Int. J. Heat Mass Transfer* **28**, 1847–1857 (1985).
12. W. P. Jones and B. E. Launder, The prediction of laminarization with a two-equation model of turbulence, *Int. J. Heat Mass Transfer* **15**, 301–314 (1972).
13. W. P. Jones and B. E. Launder, The calculation of low-Reynolds-number phenomena with a two-equation model of turbulence, *Int. J. Heat Mass Transfer* **16**, 1119–1130 (1973).
14. N. C. Markato, M. R. Malin and G. Cox, Mathematical

modeling of buoyancy-induced smoke flow in enclosures, *Int. J. Heat Mass Transfer* **25,** 63–75 (1982).
15. N. C. Markato and K. A. Pericleous, Laminar and turbulent natural convection in an enclosed cavity, *Int. J. Heat Mass Transfer* **27,** 755–772 (1984).
16. W. M. Yan and T. F. Lin, Heat transfer in buoyancy-driven flows with the simultaneous presence of laminar, transitional and turbulent flow regimes, *Wärme- und Stoffübertr.* **24,** 125–132 (1989).
17. W. M. To and J. A. C. Humphrey, Numerical simulation of buoyant, turbulent flow—I. Free convection along a heated, vertical, flat plate, *Int. J. Heat Mass Transfer* **29,** 573–592 (1986).
18. H. B. Mason and R. A. Seban, Numerical prediction for turbulent free convection from vertical surface, *Int. J. Heat Mass Transfer* **17,** 1329–1336 (1974).
19. V. C. Patel, W. Rodi and G. Scheuerer, Turbulence models for near-wall and low Reynolds number flow: a review, *AIAA J.* **23,** 1308–1319 (1985).
20. S. V. Patankar, *Numerical Heat Transfer and Fluid Flow*, Chap. 4. Hemisphere/McGraw-Hill, New York (1980).
21. W. M. Yan, Buoyancy induced heat and mass transfer in vertical channel flows, Ph.D. Thesis, Department of Mechanical Engineering, National Chiao Tung University, Hsinchu, Taiwan, January (1989).
22. J. P. Holman, *Heat Transfer*, 5th Edn, Chap. 7. McGraw-Hill, New York (1981).
23. R. J. Moffat, Contributions to the theory of single-sample uncertainty analysis, *J. Fluid Engng* **104,** 250–260 (1982).
24. S. J. Kline and F. A. McClintock, Describing uncertainties in single-sample experiments, *Mech. Engng* **75,** 3–8 (1983).
25. M. Nakajima, K. Fukui, H. Ueda and T. Mizushinal, Buoyancy effects on turbulent transport in combined free and forced convection between vertical parallel plates, *Int. J. Heat Mass Transfer* **23,** 1325–1336 (1980).
26. W. M. Yan and T. F. Lin, Buoyancy effects on low Reynolds number turbulent forced convection in vertical plate channels with symmetric or asymmetric wall temperature, *J. Chin. Soc. Mech. Engrs* **8,** 321 330 (1987).
27. P. H. Pollard and P. H. Oosthuizen, Free convection through open-ended pipes, 83-HT-68, 21st Natn. Heat Transfer Conf. (1983).
28. M. Miyamoto and M. Okayama, Study of turbulent natural convection heat transfer along a vertical plate, *Trans. Japan Soc. Mech. Engrs* (Ser. B) **48,** 490–498 (1982).
29. W. M. Yan, Y. L. Tsay and T. F. Lin, Combined heat and mass transfer in turbulent natural convection between vertical parallel plates, *Int. J. Heat Mass Transfer* **32,** 1581–1584 (1989).

APPENDIX

To estimate the uncertainties of the experimental results, the parameters and uncertainty intervals for the main contributing variables are listed in Table A1. The uncertainties of some parameters cited in Table A1 are calculated as follows:

(1) Uncertainty of temperature difference, $T_w - T_0$.

From equations (21), the difference $T'_w - T_w$, is of the order of 0.01°C in the present study. Therefore, it is reasonable to assume that the uncertainty of inner wall temperature T_w is equal to that of outer wall temperature T'_w. Thus

$$\delta(T_w - T_0) = [(\delta T_w)^2 + (\delta T_0)^2]^{1/2} = [(\delta T'_w)^2 + (\delta T_0)^2]^{1/2}. \tag{A1}$$

(2) Uncertainty of overall generating power, Q_e.

Since

$$Q_e = IV \tag{A2a}$$

$$\frac{\delta Q_e}{Q_e} = \left[\left(\frac{\delta I}{I}\right)^2 + \left(\frac{\delta V}{V}\right)^2\right]^{1/2}. \tag{A2b}$$

(3) Uncertainty of average wall heat flux, q''_w.

Since

$$q''_w = (Q_e - Q_{loss})/[\pi(R_o + R_i)l] \tag{A3a}$$

$$\frac{\delta q''_w}{q''_w} = \left\{\left[\frac{\delta(Q_e - Q_{loss})}{Q_e - Q_{loss}}\right]^2 + \left[\frac{\delta(R_o + R_i)}{R_o + R_i}\right]^2 + \left[\frac{\delta l}{l}\right]^2\right\}^{1/2} \tag{A3b}$$

where

$$\frac{\delta(Q_e - Q_{loss})}{Q_e - Q_{loss}} = \frac{1}{Q_e - Q_{loss}}[(\delta Q_e)^2 + (\delta Q_{loss})^2]^{1/2} \tag{A3c}$$

and

$$\frac{\delta(R_o + R_i)}{R_o + R_i} = \frac{1}{R_o + R_i}[(\delta R_o)^2 + (\delta R_i)^2]^{1/2}. \tag{A3d}$$

(4) Uncertainty of convective wall heat flux, q''_c.

In the analysis, the estimate of the uncertainty of q''_c is difficult. To circumvent this, we assume that q''_w and q''_c have the same uncertainty. That is to say

$$\frac{\delta q''_c}{q''_c} = \frac{\delta q''_w}{q''_w}. \tag{A4}$$

(5) Uncertainty of air properties.

The correlations utilized to represent the dependence of λ, c_p, μ and ρ on temperature are available in ref. [21]. From these correlations, we can evaluate the uncertainties of the air properties.

(6) Uncertainty of heat transfer coefficient, h

Since

$$h = q''_c/(T_w - T_0) \tag{A5a}$$

$$\frac{\delta h}{h} = \left\{\left[\frac{\delta q''_c}{q''_c}\right]^2 + \left[\frac{\delta(T_w - T_0)}{T_w - T_0}\right]^2\right\}^{1/2}. \tag{A5b}$$

(7) Uncertainty of local Nusselt number, Nu.

Since

$$Nu = \frac{hR_i}{\lambda} \tag{A6a}$$

$$\frac{\delta Nu}{Nu} = \left[\left(\frac{\delta h}{h}\right)^2 + \left(\frac{\delta R_i}{R_i}\right)^2 + \left(\frac{\delta \lambda}{\lambda}\right)^2\right]^{1/2}. \tag{A6b}$$

(8) Uncertainty of Grashof number, Gr^*

Since

$$Gr^* = \frac{g\beta q''_w R_i^5}{l\lambda\nu^2} \tag{A7a}$$

$$\frac{\delta Gr^*}{Gr^*} = \left\{\left(\frac{\delta q''_w}{q''_w}\right)^2 + \left(\frac{5\delta R_i}{R_i}\right)^2 + \left(\frac{\delta l}{l}\right)^2 + \left(\frac{\delta \lambda}{\lambda}\right)^2 + \left[\frac{\delta(g\beta/\nu^2)}{(g\beta/\nu^2)}\right]^2\right\}^{1/2}. \tag{A7b}$$

(9) Uncertainty of Rayleigh number, Ra^*.

Since

$$Ra^* = Gr \cdot Pr \tag{A8a}$$

$$\frac{\delta Ra^*}{Ra^*} = \left[\left(\frac{\delta Gr^*}{Gr^*}\right)^2 + \left(\frac{\delta Pr}{Pr}\right)^2\right]^{1/2}. \tag{A8b}$$

Table A1. Parameters and estimated uncertainties for heat transfer

Parameter	Nominal value	Uncertainty
R_i (m)	0.03–0.05	±0.0005 m
l (m)	1.2–2.8	±0.0005
T_0 (°C)	27–34	±0.2°C
T_w'' (°C)	32–200	±0.2°C
$T_w - T_0$ (°C)	5–170	±0.2828°C
I (A)	40–300	±1%
V (V)	0.1–1.2	±1%
Q_e (W)	5–300	±1.414%
Q_{loss} (W)	0.8–40	±10%
q_w'' (W m^{-2})	20–300	±4.24%
q_e'' (W m^{-2})	20–300	±4.24%
λ (W m^{-2})	0.0261–0.0363	±0.05%
c_p (J kg^{-1} °C^{-1})	1.005×10^3–1.02×10^3	±0.1%
μ (N m s^{-2})	18.53×10^{-6}–24.93×10^{-6}	±0.4%
ρ (kg m^{-3})	0.784–1.165	±0.06%
$g\beta/\nu^2$ (m^{-3})	2.16×10^7–1.32×10^8	±0.809%
Pr	0.70–0.71	±0.415%
Calculated uncertainty in $\overline{Nu}$: 4.40–5.53%		
Calculated uncertainty in Ra^*: 6.63–9.40%		

ETUDE THEORIQUE ET EXPERIMENTALE DES ECOULEMENTS DE CONVECTION NATURELLE A GRAND NOMBRE DE RAYLEIGH DANS LES TUBES

Résumé—Une étude théorique et expérimentale est conduite sur les écoulements de convection naturelle dans les tubes à grand nombre de Rayleigh. Les effets de la conduction dans la paroi et les variations des propriétés thermiques du fluide et du tuyau sont considérés. Un modèle de turbulence k–ε à faible nombre de Reynolds est utilisé pour traiter les régimes de transition et de turbulence en incluant les effets de flottement. Les distributions de température pariétale et de nombre de Nusselt calculés et mesurés sont en bon accord. Des formules empiriques pour le débit induit et le nombre de Nusselt moyen sont proposées. Les résultats montrent que les caractéristiques du transfert par convection naturelle dans un tube vertical approchent celles d'un plan vertical unique pour les grands nombres de Rayleigh.

THEORETISCHE UND EXPERIMENTELLE UNTERSUCHUNG DER NATÜRLICHEN KONVEKTION IN EINEM ROHR BEI HÖHEREN RAYLEIGH-ZAHLEN

Zusammenfassung—Die natürliche Konvektion in Rohren wird bei höheren Rayleigh-Zahlen sowohl theoretisch wie auch experimentell untersucht. In dieser Betrachtung sind Wärmeleiteffekte in der Rohrwand wie auch temperaturabhängige Stoffeigenschaften von Fluid und Rohrwand berücksichtigt. Zur Berechnung der Auftriebsströmung im Übergangs- und im turbulenten Bereich wird ein k–ε-Turbulenzmodell für kleine Reynolds-Zahlen verwendet. Berechnete und gemessene Verteilung von Wandtemperatur und Nusselt-Zahl stimmen gut überein. Es werden empirische Korrelationen für den induzierten Massenstrom und für die mittlere Nusselt-Zahl vorgeschlagen. Die Ergebnisse zeigen, daß der Wärmeübergang durch natürliche Konvektion in einem senkrechten Rohr demjenigen an einer einzelnen senkrechten Platte bei großen Rayleigh-Zahlen ähnlich ist.

ТЕОРЕТИЧЕСКОЕ И ЭКСПЕРИМЕНТАЛЬНОЕ ИССЛЕДОВАНИЕ ЕСТЕСТВЕННОКОНВЕКТИВНЫХ ТЕЧЕНИЙ В ТРУБАХ ПРИ ВЫСОКИХ ЧИСЛАХ РЭЛЕЯ

Аннотация—Теоретически и экспериментально исследуются естественноконвективные течения в трубах при высоком числе Рэлея. Анализируются также эффекты теплопроводности стенки, температурной зависимости характеристик жидкости и стенки трубы. Переходный и турбулентный режимы течения с учетом действия подъемной силы изучаются на основе k–ε модели турбулентности для области низких чисел Рейнольдса. Получено хорошее согласие между теоретическими и экспериментальными распределениями температуры на стенке и значениями числа Нуссельта. Предложены эмпирические соотношения для расчета скорости возбуждаемого течения и среднего числа Нуссельта. Результаты показывают, что характеристики естественноконвективного теплопереноса в вертикальной трубе близки к теплопереносу от одиночной вертикальной пластины при большом числе Рэлея.